The TanDEM-X Digital Elevation Model and Terrestrial Impact Structures

Manfred Gottwald, Thomas Kenkmann, Wolf Uwe Reimold, Thomas Fritz, and Helko Breit

***Abstract*—We utilized the TanDEM-X digital elevation model (DEM) for investigating the complete record of confirmed terrestrial impact structures with respect to its suitability to support geological analysis. The consistently high resolution and high accuracy of this model is a prerequisite for detailed morphological studies. This DEM represents an interesting repository to aid in preparing and executing fieldwork for the exploration of new impact crater candidates. For a selection of small, mid-sized, and large impact structures, we here compare the TanDEM-X results with those from other DEMs that were derived either with synthetic aperture radar interferometry or from optical stereo pairs. Our analysis includes high-resolution mapping and the generation of detailed elevation cross sections. Only for very small impact craters, when the diameter is in the order of the pixel posting of TanDEM-X of 12 m or when the texture of the local environment does not support radar remote sensing, accurate analysis is hampered. Our results demonstrate that the high horizontal and vertical accuracies of the TanDEM-X DEM, coupled with its dense pixel grid, provide a considerable improvement in space-borne remote sensing of the complete record of simple and complex terrestrial impact structures over a wide range of diameters.**

***Index Terms*—Digital elevation model (DEM), impact geology, impact structures, radar interferometry, TanDEM-X, terrain mapping.**

I. Introduction

IMPACT cratering has been a fundamental process onto the solid surfaces of large and small bodies in the solar system. This process took place at a high rate in the distant past and has been approximately constant over the last 3×10^9 yr. Even today, the number of small bodies orbiting the Sun between the large planets counts in the millions. Almost 23 000 asteroids have been classified as near-earth asteroids, supplemented by slightly more than one hundred near-earth comets. This is, however, only a small fraction of the estimated total number of small bodies entering the inner solar system. Among such *near-earth objects (NEOs)* are bodies that may approach the earth even further. These so-called *potentially hazardous objects (PHOs)* have a *minimum-orbit-intersection distance* with the earth of $< 7.5 \times 10^6$ km and their brightness can be translated into an approximate diameter of at least 140 m. At the time of writing, more than 2000 PHOs have been identified (e.g., [1] and references therein). Ongoing sky surveys continuously increase the numbers of both NEOs and PHOs.

When such an object collides with the earth, this occurs with hypervelocities of more than 11.2 km·s^{-1}. Hypervelocity impacts are unique because of the following:

1) Their enormous energy release, i.e., the energy as defined by the impactor's kinetic energy.
2) The highly dynamic effects of the collision, e.g., a crater of 1 km forms in just a few seconds, and even the world's largest known impact structure, Vredefort in South Africa with an original diameter of at least 250 km, was produced in only 15 min.
3) Their energy release is almost point like.
4) Their extreme pressures and temperatures, up to hundreds of GPa and thousands of °C.
5) The relative rarity of events.

The extreme conditions at impact, in the upper crust of a planet, cannot be produced by other geological phenomena. These ultrahigh pressures and temperatures cause unique shock-metamorphic effects in the target rock that are regarded as unambiguous, diagnostic recognition criteria of impact structures. Detecting such evidence for shock deformation provides the only established criterion for the confirmation of a suspected impact structure, besides unambiguous proof of meteoritic material, derived from the extraterrestrial impactor, at the impact site (see [2]). Therefore, impact structure detection always requires appropriate fieldwork, followed by meticulous petrographic and geochemical studies.

Space-borne remote sensing can support impact studies in many ways [3]. For impact structures that cannot be explored by fieldwork because of their remote or difficult location, basic properties can be derived from remote sensing data. In addition, the investigation of certain structures via remote sensing can deliver supplemental information, for example, imaging in ultraviolet to infrared wavelengths and microwave (radar) bands can provide knowledge about the surface composition or elevation information. The design of earth observation missions in polar

Manuscript received June 9, 2020; revised February 26, 2021; accepted March 22, 2021. Date of publication March 30, 2021; date of current version April 26, 2021. The work of Wolf Uwe Reimold was supported in part by a Brazilian National Council for Scientific and Technological Development (CNPq) Fellowship under Grant 305761/2019-6 and in part by the Coordenação de Aperfeiçoamento de Pessoal de Nivel Superior—Brasil—Finance Code 001. *(Corresponding author: Manfred Gottwald.)*

Manfred Gottwald, Thomas Fritz, and Helko Breit are with the German Aerospace Center, Remote Sensing Technology Institute, 82234 Wessling, Germany (e-mail: manfred.gottwald@gmail.com; thomas.fritz@dlr.de; helko.breit@dlr.de).

Thomas Kenkmann is with the Institute of Earth and Environmental Sciences—Geology, Albert-Ludwigs-Universität Freiburg, 79104 Freiburg im Breisgau, Germany (e-mail: thomas.kenkmann@geologie.uni-freiburg.de).

Wolf Uwe Reimold is with the Geochronology and Isotope Geochemistry Laboratory, Institute of Geosciences, University of Brasilia, Brasilia CEP 70910-900, Brazil (e-mail: wolf.uwer@gmail.com).

Digital Object Identifier 10.1109/JSTARS.2021.3069640

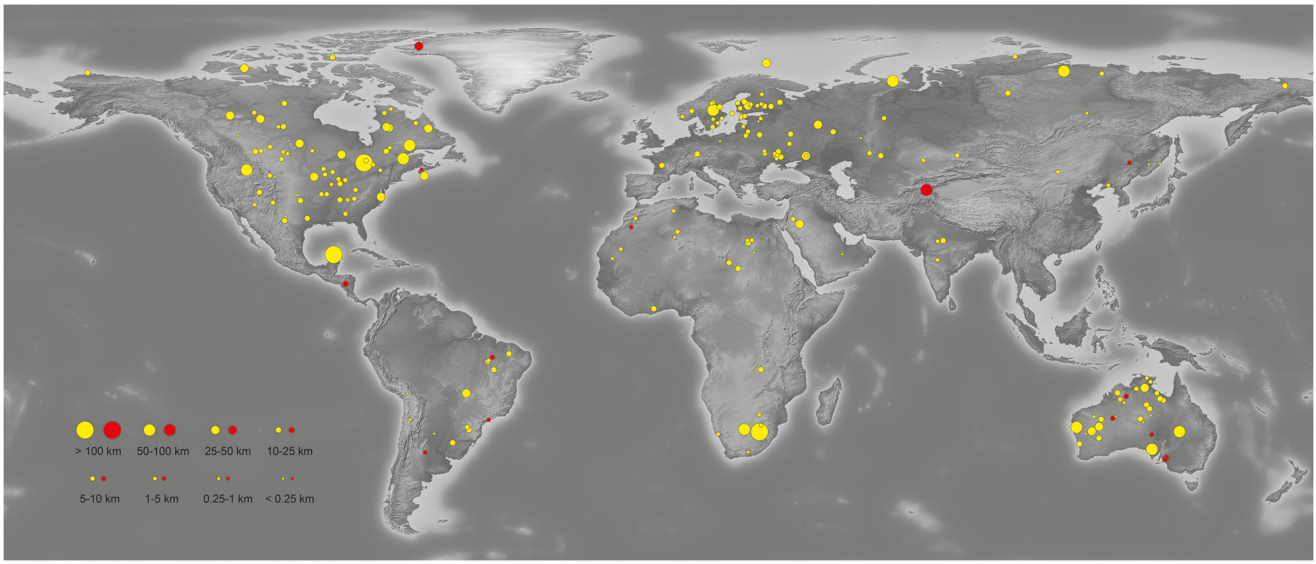

Fig. 1. Record of terrestrial impact structures. The sizes of the symbols denote the diameter of each structure. Yellow symbols show confirmed impact structures, whereas red symbols indicate those where further confirmation is required.

orbits and with sensors with a wide field-of-view usually ensure coverage of the entire globe on short timescales.

II. Record of Terrestrial Impact Structures

Earth is a highly dynamic planet, whose surface has been and still is continuously modified. Plate tectonics, erosion, and sedimentation/burial have changed our planet's face over geological periods and epochs. On shorter time scales, volcanism, earthquakes, and tsunamis have modified its topography. The majority—about 2/3—of the terrestrial surface is covered by oceanic basins, with the seafloor having a maximum age of only about 200×10^6 years. This relatively young crust does not provide an extensive archive for the earth's geological past. This is different from the surfaces of many other solar system bodies that lack a dense atmosphere and open water. On their surfaces, a plethora of impact structures could accumulate with time and permits insights into the early history of these bodies.

For earth, the active geological processes affecting the crust have erased most of the scars of previous impacts. A recent compilation (see [1]) lists 194 impact structures with confirmation based on the strict criteria of shock-metamorphism, and another 14 structures where confirmation is still ambiguous or requires further work (see Fig. 1). This atlas includes topographic maps, generated from the TanDEM-X DEM, together with fact sheets describing the impact geology and the currently established parameters such as diameters and ages for each of these impact structures. The majority of confirmed impact structures are found in North America, Europe, and Australia; considerably less have been detected in Asia, Africa, and South America. One reason for this is that on the former continents a larger fraction of the earth's crust dates back to Archean or early Proterozoic times. Another cause is the fact that on some continents, extensive space research and geological exploration have been undertaken already for some time, and impact cratering studies have been pursued particularly by some highly motivated individuals. This is in contrast to the regions deficient in impact structures, where studies have been hampered by access limitations, such as in vast areas of rainforest or in those countries with safety concerns.

The preservation status of the terrestrial impact structures differs, obviously as a function of their relative ages. Usually small simple craters of relatively young age still display the typical bowl-shaped depression with an elevated rim, whereas erosion may have considerably modified the morphology of larger structures with complex morphologies (see [4]). The central uplift, a typical morphological feature of complex craters, often has only remained as a deeply eroded relic. Sometimes the impact structure has been completely erased and the impact exposure is limited to outcrops of impact lithologies, without any traces of the original topography. A large fraction of the sample of terrestrial impact structures is buried below younger rock formations and/or submerged in lakes or oceans. These can only be studied by drilling or geophysical methods.

The smallest listed single crater structures on earth are Sterlitamak in Russia with 9.4 m diameter (see [1]), which was erased during exploration, and Carancas in Peru with a diameter of 14.2 m (see [1]). Vredefort in South Africa counts as the largest confirmed impact structure with an original diameter of at least 250 km (see [1]). The majority of terrestrial impact structures can be found in the diameter range from 1 to 25 km (see Table I).

The ages of impact structures are usually derived from radiometric dating or from stratigraphic and paleontological constraints. Eyewitness reports exist for the youngest impact events that occurred in 2007 in Peru (Carancas) and 1998 in Russia (Sterlitamak). Also, the Sikhote Alin meteorite fall from 1947, which created a strewn field of small craters, was observed by the local population. At the opposite end of the age scale, several structures date back to Paleoproterozoic times, including Vredefort in South Africa with an age of $2.023 \pm 0.004 \times 10^9$ yr (see [1]) and Yarrabubba in Australia that has recently been

TABLE I
CURRENT STATISTICS OF TERRESTRIAL IMPACT STRUCTURES

	Africa [a]	North/Central America	South America	Asia	Australia	Europe
Impact structures						
Confirmed	20	62	11	21	26	54
Further confirmation required	1	3	3	2	5	0
Diameter (km)						
< 0.25	1	4	2	3	4	4
0.25-1	3	1	1	1	2	1
1-5	8	9	3	5	3	19
5-10	1	20	2	6	6	11
10-25	5	16	5	5	10	12
25-50	0	9	1	1	3	5
50-100	1	3	0	1	3	2
> 100	1	3	0	1	0	0

[a]One impact structure with an unknown diameter.

TABLE II
CHARACTERISTICS OF GLOBAL SPACE-BORNE DEMS

	TanDEM-X	SRTM	ALOS AW3D30	ASTER GDEM V3
Data acquisition	Dec 2010 – early 2015	Feb 11-22, 2000	Jan 2006 – Apr 2011	Mar 2000 – Nov 2013
Instrument	radar X-band / 3.1 cm	radar C-band / 5.6 cm	optical / 0.52-0.77 μm	optical / 0.78-0.86 μm
Coverage	global	56°S – 60°N	global	global
Pixel posting (m)	12 m	30 m	30 m	30 m
Absolute accuracy (specified)				
Horizontal	< 10 m	20 m	unspecified	30 m
Vertical	< 10 m	16 m	unspecified	17 m
Datum				
Horizontal	WGS84	WGS84	WGS84	WGS84
Vertical	WGS84[a]	EGM96	EGM96	EGM96

[a]WGS84 elevations have been transferred to EGM96 elevations for the studied scenes.

dated to $2.246 \pm 0.017 \times 10^9$ yr (see [1]). Older evidence of impact in the earth's rock record exists only through a number of so-called *impact spherule layers* that represent distal impact ejecta of up to Neoarchean age of $\sim 3.2–3.4 \times 10^9$ yr ([5]).

Small impact craters are usually young, as erosion may quickly erase their topography. This is also true for eight of the nine known strewn fields of small impact craters. The Douglas crater field in Wyoming, North America, however, has a Permian age of 280×10^6 yr (see [1]). Relatively shortly after the corresponding impact, rapid burial must have preserved these small craters. This was followed by later exhumation of the craterls, which made them visible again.

The current number of confirmed impact structures certainly does not represent the full record of terrestrial impact structures. New structures have been added at a rate of about 2–3 per year. Estimates of the number of terrestrial impact structures still undiscovered suggest that about 350 are still missing in the diameter range from 0.25 to 6 km (see [6]).

III. IMPACT STRUCTURE MAPPING WITH DIGITAL ELEVATION MODELS (DEMS)

The provision of accurate elevation information on a global scale is a particular asset of space-borne remote sensing of the earth. A DEM can either be derived from optical stereo pairs or radar data obtained in interferometric mode. Optical sensors require a cloud-free atmosphere with a sunlit scene for data acquisition, whereas synthetic aperture radar (SAR) interferometry is not compromised by such effects. Artifacts introduced by the SAR method and its interferometric application can be minimized through an appropriate mission design, together with careful calibration and DEM extraction during data processing.

Precise remote sensing mapping is a prerequisite for detailed studies of a particular impact structure. It provides its morphology, yields insight into its local and regional topographic context, and can facilitate the preparation of on-site campaigns.

We applied the TanDEM-X DEM (see [7] and [8]) to map the sites of all currently confirmed terrestrial impact structures. For certain impact structures, three other global DEMs, available for public access, were used for comparison. The shuttle radar topography mission (SRTM), a joint project of NASA, DLR, and ASI (the U.S., German, and Italian Space Agencies, respectively), acquired SAR interferometric data of the land surfaces in early 2000 with a C-band and an X-band sensor (see [9]). The resulting 1" SRTM C-band DEM covers the area from 56 °S to 60 °N that was within the reach of the selected shuttle orbit. The ALOS AW3D30 DEM is a derivative of AW3D, the commercially available DSM with a pixel posting of 5 m that was obtained from optical stereo pairs taken with the panchromatic stereo mapping sensor PRISM aboard the Advanced Land Observing Satellite (ALOS, [10]). Optical stereo pairs from the Advanced Spaceborne Thermal Emission and Reflection Radiometer (ASTER) are the source of the ASTER GDEM, which is now available in its third

TABLE III
COMPARISON OF IMPACT STRUCTURE DEM—FULL SCENE

	Minimum elevation (m)	Mean elevation ± Std Dev (m)	Maximum elevation (m)
Manicouagan			
TanDEM-X	261.9	533.0 ± 139.1	1107.8
SRTM	295.0	526.7 ± 140.5	1099.0
ALOS	234.0	528.7 ± 140.9	1110.0
ASTER	287.0	523.8 ± 140.8	1101.0
Serra da Cangalha			
TanDEM-X	218.7	344.3 ± 54.1	646.4
SRTM	229.0	346.5 ± 53.2	647.0
ALOS	230.0	347.2 ± 53.6	644.0
ASTER	217.0	340.1 ± 53.6	645.0
Talemzane			
TanDEM-X	562.0	630.2 ± 22.4	680.9
SRTM	562.0	631.6 ± 21.8	685.0
ALOS	566.0	633.7 ± 21.5	688.0
ASTER	539.0	634.1 ± 24.9	731.0

TABLE IV
COMPARISON OF IMPACT STRUCTURE DEM—TRANSECT

	Mean elevation difference (m)	RMSE [a] (m)
Manicouagan		
TanDEM-X – SRTM	1.65	10.98
TanDEM-X – ALOS	-0.73	8.76
TanDEM-X – ASTER	4.62	11.07
Serra da Cangalha		
TanDEM-X – SRTM	-1.93	9.30
TanDEM-X – ALOS	-1.57	8.57
TanDEM-X – ASTER	3.94	10.30
Talemzane		
TanDEM-X – SRTM	-0.25	2.68
TanDEM-X – ALOS	-1.79	2.98
TanDEM-X – ASTER	1.34	7.64

[a]Root-mean-square error

version [11]. The specifications of all four DEMs are summarized in Table II.

On local and regional scales, digital terrain models, usually derived from airborne LiDAR measurements, are supplemental sources for impact structure mapping with very high horizontal and vertical resolution. Their limited extent often restricts their application to small craters or crater fields. Elevations determined by LiDAR refer to "bare earth" and do not reflect vegetation or buildings. This is different from elevation data from space-borne sensors. For the radar X-band, the first backscattered signal is close to the top of the vegetation, i.e., the tree canopy in forest areas.

Properties of an impact structure, such as location and size, define how suitable a certain DEM is for its mapping. As we studied DEMs with an independent pixel posting of 12 m and higher, the detectability of very small craters is limited. This is particularly true in an environment where strong vegetation shields the impact crater from the impinging radiation of the space-borne remote sensing instrument.

Fig. 2. Manicouagan in a Copernicus Sentinel-2 RGB image, fused with a hillshaded TanDEM-X DEM. The Sentinel-2 data were acquired on August 31, 2018.

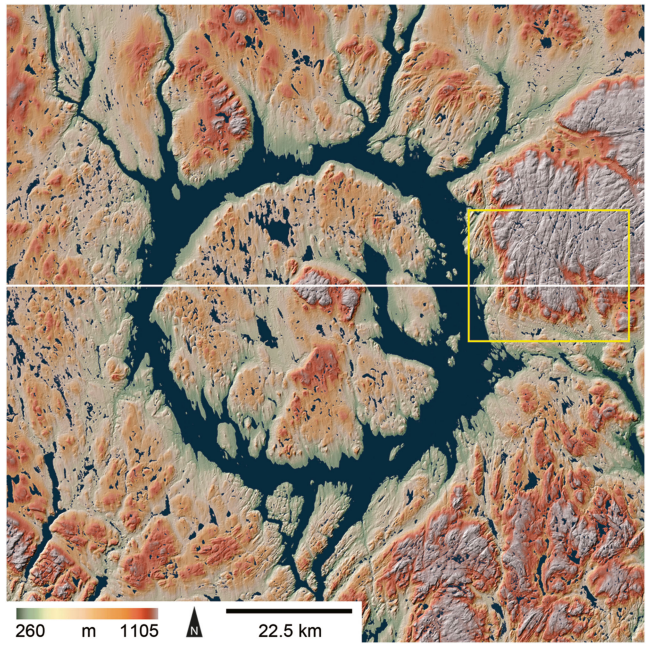

Fig. 3. Manicouagan in a color-coded, hillshaded TanDEM-X DEM, supplemented by a water mask. The yellow box denotes the area used for DEM comparison in Fig. 4, whereas the white horizontal line indicates the transect of Fig. 5.

Here, we selected three impact structures of different sizes and locations for a detailed comparison of the suitability of different DEMs for impact crater studies: Manicouagan in Canada as an example for a large complex structure, Serra da Cangalha in Brazil as a mid-sized complex structure, and Talemzane in Algeria as an example for a small simple impact crater. The absolute height accuracy at 90% confidence level (see [8]) for

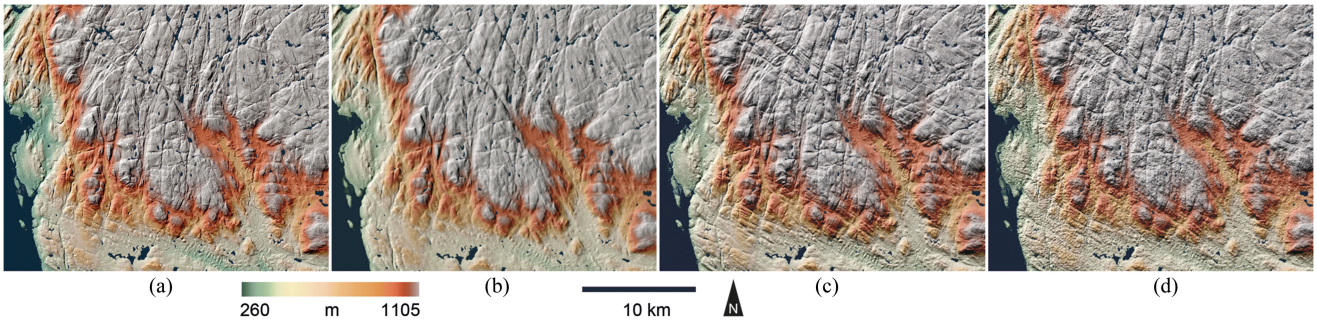

Fig. 4. An area east of the Manicouagan reservoir displayed at identical resolution with (a) TanDEM-X, (b) SRTM, (c) ALOS, and (d) ASTER. The color-coded hillshaded map was produced from the corresponding DEMs using the same workflow.

these structures has been derived at < 5 m (Manicouagan) and $<$ 2 m (Serra da Cangalha and Talemzane). Statistics with a minimum, maximum, and mean elevation with standard deviation for the full DEM scenes of the three impact structures are given in Table III. Table IV presents the mean elevation difference and the standard root-mean-square error (RMSE) along the respective west-east transects. In order to allow direct comparison between the transect elevations, the TanDEM-X DEM was resampled to a pixel posting identical to that of the other space-borne DEMs.

A. Manicouagan

Manicouagan in Quebec, Canada (lat $=$ 51°23′N, long $=$ 68°41′W) is a 214 $\times$ 10^6 yr old complex impact structure with a diameter of 100 km (see [12]). Manicouagan lies about 200 km northwest of the mouth of the St. Lawrence River in a hilly environment with numerous lakes and dense boreal vegetation. A prominent feature is the annular Manicouagan Reservoir, dammed up by the Daniel–Johnson dam in the south (see Figs. 2 and 3). This reservoir makes Manicouagan one of the very few impact structures clearly visible from space. The outer diameter of this reservoir measures 65 km. Inside of the reservoir follows an inner plateau with the centermost area being occupied by a 25 km wide remnant of the central uplift; its highest elevation is known as Mont de Babel. The water mask for Manicouagan is derived from the TanDEM-X radar amplitude image, complemented by the water mask delivered as part of the TanDEM-X auxiliary data. Because the level of the reservoir cycles by 3–7 m throughout a year with absolute values having varied between ∼340 and 350 m elevation since the year 2000, the DEMs considered here may display slightly different topography along the reservoir's shorelines. Due to the fact that the tree canopy provides the first backscattered signal, the timespan of data acquisition for DEM generation may also be reflected in absolute elevation levels in areas with dense vegetation.

For comparison of the TanDEM-X data with the three DEMs, we selected a 23.7 $\times$ 29 km large area east of the reservoir. In Fig. 4, this area is shown for all four DEMs. Although the print scale does not allow displaying the impact structure in full resolution, it is already obvious for this large area that TanDEM-X provides the finest detail. ALOS AW3D30 slightly outperforms SRTM, whereas in the ASTER GDEM V3 elevation noise is already apparent.

Minimum and maximum elevations determined by the four methods are presented in Table III. They differ considerably by up to 61 m. This is not surprising for a scene in a rugged environment with an extent of 115 $\times$ 115 km, and for which the corresponding DEMs were generated with two different methods. The mean elevations are in much better agreement and comply well with the specified absolute vertical error (see Table II). A west-east transect through Manicouagan, and across Mont de Babel, is shown in Fig. 5, together with the elevation differences between the four DEMs. All four DEMs outline the overall morphology of the impact structure along the transect in a similar manner. The mean elevation difference is largest for ASTER, but it is in agreement with the accumulated absolute height accuracy with 90% linear error of TanDEM-X (see Table IV and [8]). Large excursions in elevation differences occur mainly where the slope of the terrain is high.

B. Serra Da Cangalha

Serra da Cangalha in Tocantins State, Brazil (lat $=$ 08°05′S, long $=$ 46°51′W) is a complex impact structure with a diameter of 13.7 km and an age younger than 300 $\times$ 10^6 yr (see [13]). It is considerably eroded but still shows a remarkable morphology (see Fig. 6). From the center outward, several ring-like features can be distinguished, caused by selective erosion of tilted strata. Most prominent is an up to 350 m high collar surrounding the innermost depression. These features correspond to the central uplift of this impact structure. The region of Serra da Cangalha is densely vegetated comprising tropical savanna with riparian forests. Serra de Cangalha was already studied in the past using the SRTM DEM (see [14]).

We analyzed the Serra da Cangalha impact structure in the same manner as Manicouagan. The corresponding hill-shaded topographic TanDEM-X map is displayed in Fig. 7. This scene covers an area of 34 $\times$ 34 km. A 9 $\times$ 7.5 km wide section of the northeast quadrant of the impact structure was used for comparing the four DEMs (see Fig. 8). As in the case of Manicouagan, TanDEM-X allowed us to map the scene with the finest detail. Even vegetation patches and rural roads can be discerned. In the collar surrounding the central depression, the topographic fine structure is obvious. This is not the case for the

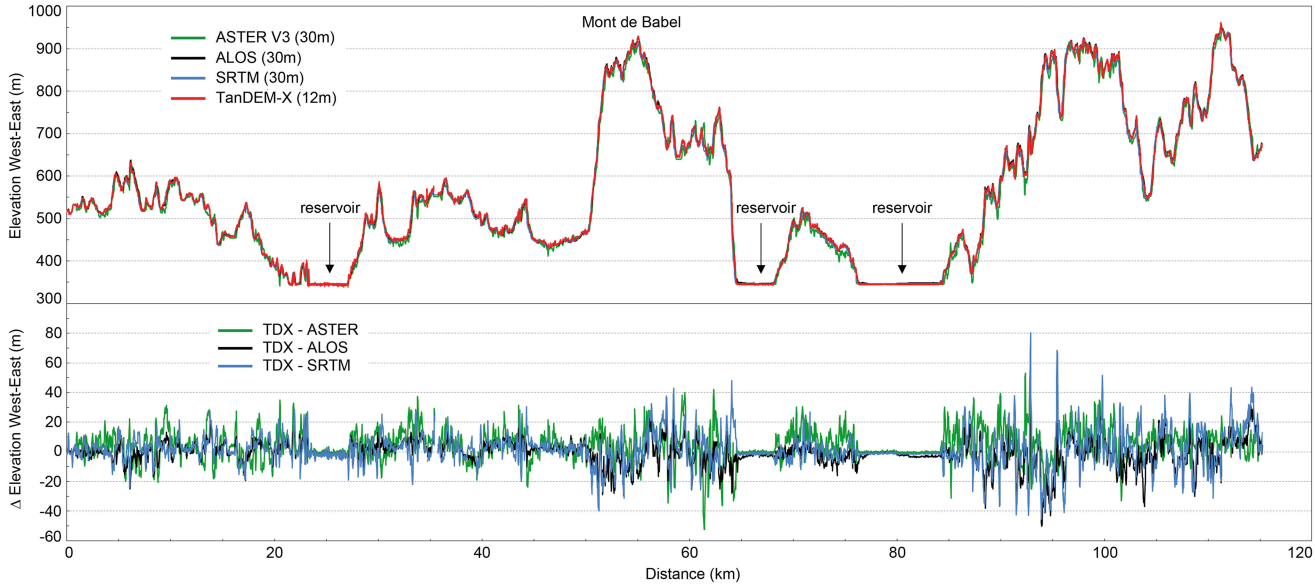

Fig. 5. West-east transect through the Manicouagan impact structure based on four space-borne DEMs. The top display shows the elevation profile, whereas the bottom display indicates the elevation differences compared to TanDEM-X, which was resampled to a pixel posting of 30 m.

Fig. 6. Serra da Cangalha in a Copernicus Sentinel-2 RGB image, fused with a hillshaded TanDEM-X DEM. The Sentinel-2 data were acquired on August 31, 2018.

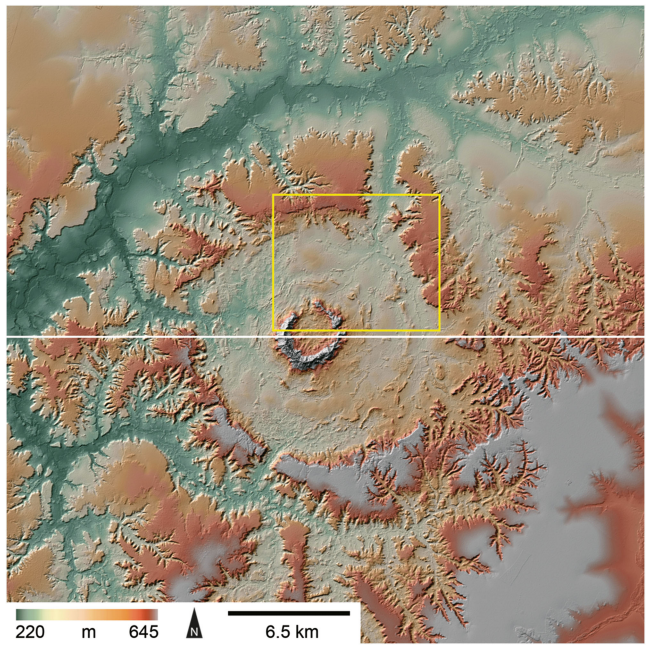

Fig. 7. Serra da Cangalha in a color-coded hillshaded TanDEM-X DEM. The yellow box denotes the area used for DEM comparison in Fig. 8, whereas the white horizontal line indicates the transect of Fig. 9.

displays produced with the other DEMs. None of these permits the detection of much detail in the shallow terrain between the collar and the outer ring that corresponds to the crater rim. Most obvious is the apparent elevation noise in the ASTER GDEM V3. ALOS has again a slight edge over SRTM.

Since the scene for Serra da Cangalha is considerably smaller, with the elevation range being only about 50% of that for Manicouagan, already the minimum/maximum elevations in Table III extracted from the DEMs agree quite well with the mean elevations being compliant with the specified absolute vertical error (see Table II). The west-east transect extends across the center of Serra de Cangalha. The collar, crater rim, and intermediate rings (see [13]) are visible in all four DEMs (see Fig. 9). As for Manicouagan, the ASTER GDEM V3 tends to provide slightly lower (by about 4 m) elevations. The maximum differences between TanDEM-X and the other results occur where the transect indicates steep slopes, particularly over the collar.

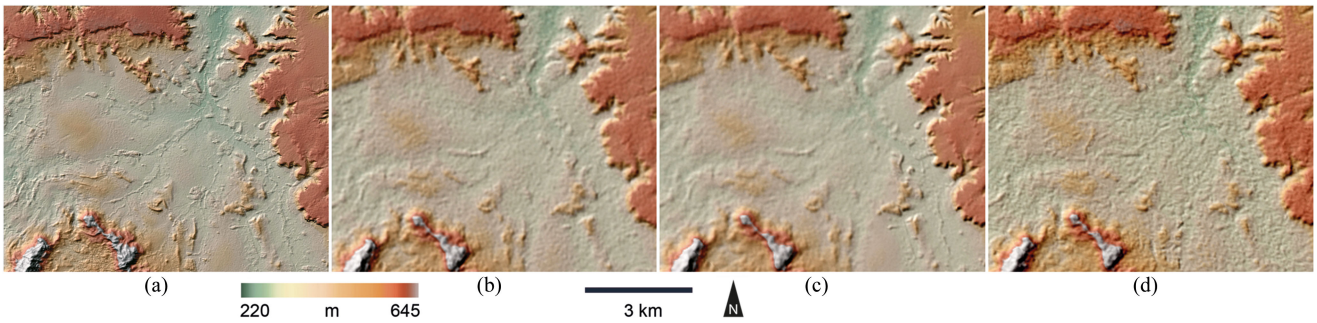

Fig. 8. Northeast quadrant of the Serra de Cangalha impact structure, displayed at identical resolution with (a) TanDEM-X, (b) SRTM, (c) ALOS, and (d) ASTER. The color-coded hillshaded map was produced from the corresponding DEMs using the same workflow.

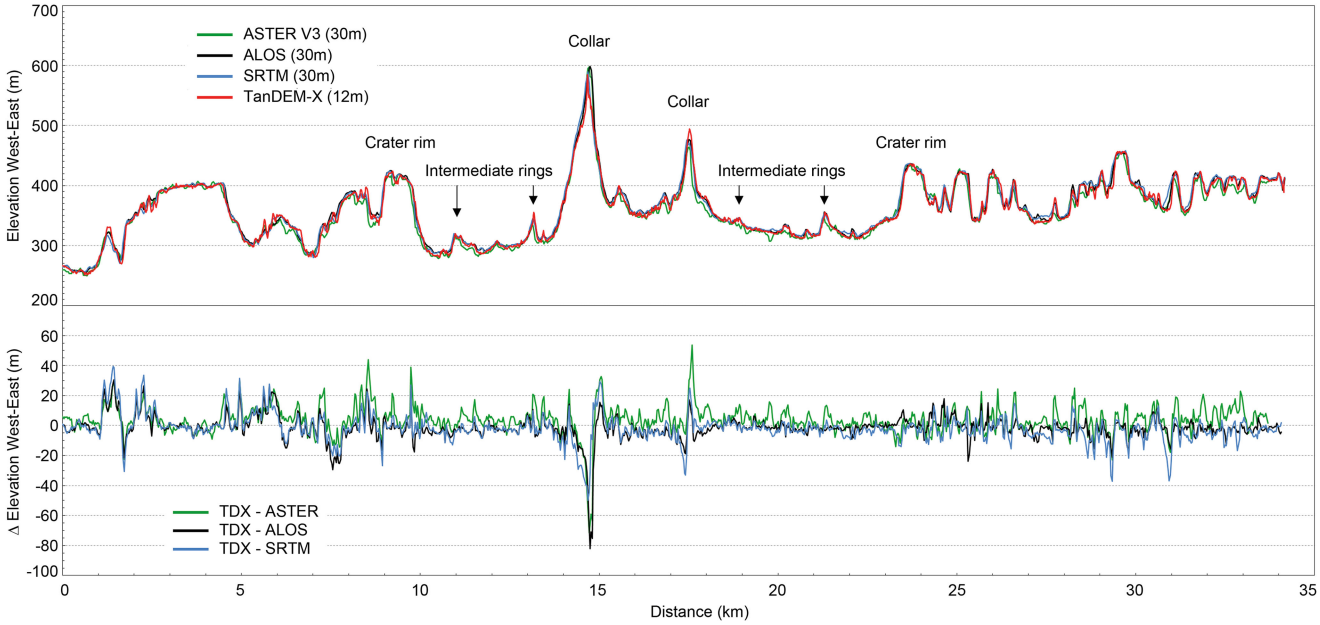

Fig. 9. West-east transect through the Serra da Cangalha impact structure based on four space-borne DEMs. The top display shows the elevation profile, whereas the bottom display indicates the elevation differences compared to TanDEM-X, which was resampled to a pixel posting of 30 m.

C. *Talemzane*

Talemzane is a simple impact crater with a diameter of 1.75 km in Laghouat Province, Algeria (see [15]), at the northern edge of the Sahara (lat = 33°19′N, long = 04°02′E). The crater's age is estimated between 0.5×10^6 and 3×10^6 yr. The vicinity of the crater is an arid desert landscape. Immediately to the west runs the wadi *Attar Qued*, whereas further to the west and north, the land surface begins to gently rise. Talemzane was the first impact crater detected with a space-borne radar imaging device, when SIR-A, NASA's first Shuttle radar mission from 1981, showed it as a feature in its data (see [16]).

Talemzane was analyzed in the same way as Manicouagan and Serra de Cangalha. The Talemzane scene with an extent of 17.5 × 17.5 km is shown in Figs. 10 and 11. Its central part with a width of 5.5 × 4.5 km was used for DEM comparison (see Fig. 12). Now the superior pixel posting of the TanDEM-X DEM becomes readily apparent.

The TanDEM-X DEM permits detailed mapping of Talemzane's morphology, including gullies representing the small drainage network terminating in the crater depression. Even hints of a remnant ejecta blanket emanating from the crater rim can be discerned. The elevation noise in the southern part of the crater depression results from the presence of desert shrubs. Wadi *Attar Oued* to the west of the crater shows a distinct outline. In all other maps, this level of detail is not present, whereas the ALOS map still appears slightly more detailed than the SRTM map, artifacts have already become obvious. In the ASTER map, detection of the crater rim and depression is considerably hampered by the presence of high elevation noise and artifacts. The flat terrain around Talemzane challenges deriving elevations from optical stereo pairs.

The range of elevations for the Talemzane scene covers only 70 m. Minimum and maximum values agree reasonably well between TanDEM-X and SRTM, whereas the two DEMs obtained from optical stereo pairs, particularly the ASTER GDEM

Fig. 10. Talemzane in a Copernicus Sentinel-2 RGB image, fused with a hillshaded TanDEM-X DEM. The Sentinel-2 data were acquired on September 2, 2018.

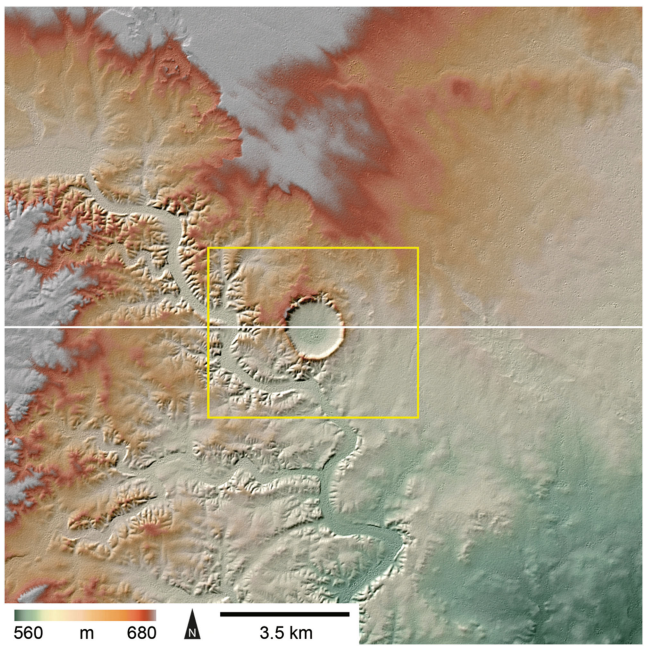

Fig. 11. Talemzane in a color-coded hillshaded TanDEM-X DEM. The yellow box denotes the area used for DEM comparison in Fig. 12, whereas the white horizontal line indicates the transect of Fig. 13.

V3, show larger deviations (see Table III). High elevation noise, coupled with artifacts, in the ASTER GDEM V3 is also obvious throughout the west-east transect (see Fig. 13) and manifests itself in a large RMSE (see Table IV).

IV. TanDEM-X Impact Record

Meanwhile, we have studied the full record of confirmed terrestrial impact structures using the final TanDEM-X DEM (see [1]). Previous work (see [17]) was based on individual acquisitions using the TanDEM-X Raw DEMs that were the source for generating the mosaicked final DEM (see [18] and [19]). Even these digital elevation data proved to be a major step forward in mapping the morphology of terrestrial impact structures when comparing them to the SRTM and ASTER GDEM V2. It is obvious in Figs. 8 and 12 that mapping impact structures with the 30 m DEMs introduces some kind of fuzziness beyond a certain image scale. It becomes particularly dominant when elevation noise and artifacts are present, as for Talemzane. The TanDEM-X DEM, however, permits detailed mapping even in this case. Only for impact craters with very small diameters, the TanDEM-X DEM begins to display some softness for the selected image scale (see Figs. 14–16).

A total of 194 impact structures are considered confirmed and can be classified as follows: 108 show significant topography, whereas the rest is either buried underground, erased, or, in addition, submerged under large water bodies. Of the remaining 14 where further confirmation is required, 10 are visible in topography and only 4 are hidden from view because they are buried or eroded.

Challenges in exploiting the TanDEM-X DEM for impact structure studies exist for very small craters where the pixel posting of 12 m, coupled with complex radar backscatter properties due to vegetation or sand, becomes the limiting factor. Additionally, even for larger impact structures, in areas where the landscape exhibits steep slopes and canyon-like features, the SAR method and its interferometric application can be hampered by the sideways-looking technique and the resulting ambiguous or shadowed range measurements. This applies particularly to Upheaval Dome in Utah's Canyonlands National Park and the Ritland structure at Norway's fjord-dissected west coast.

A total of 18 known impacts have left an imprint on the earth's surface with diameters < 250 m. With the exception of the Haviland crater in Kansas/USA and Sterlitamak in Russia, which have meanwhile been destroyed by anthropogenic activity, these structures are still recognizable in topography. Often they form fields of small impact craters because the incoming meteoroid broke up in the atmosphere and caused a meteorite to fall.

The young Kamil crater in Egypt with a diameter of 45 m is the smallest detectable impact crater in the TanDEM-X DEM (see Fig. 14). It is located in the Libyan Desert in a rocky environment. This setting provides well-suited conditions for the detection of a feature that is only 3.6 TanDEM-X DEM pixels wide. Although craters of this size are still too small to allow a detailed study of their morphologies using the TanDEM-X elevation data, Kamil proves the high quality of these data.

Another example is the Henbury crater field. It lies in Australia's Northern Territory in an arid region with occasional vegetation patches and comprises 12–16 crater pits ranging in diameter from 6 to 180 m and in depth up to 15 m. The Henbury craters are slightly older than Kamil. Their original sharp outlines, thus, have been softened by erosion. Several of

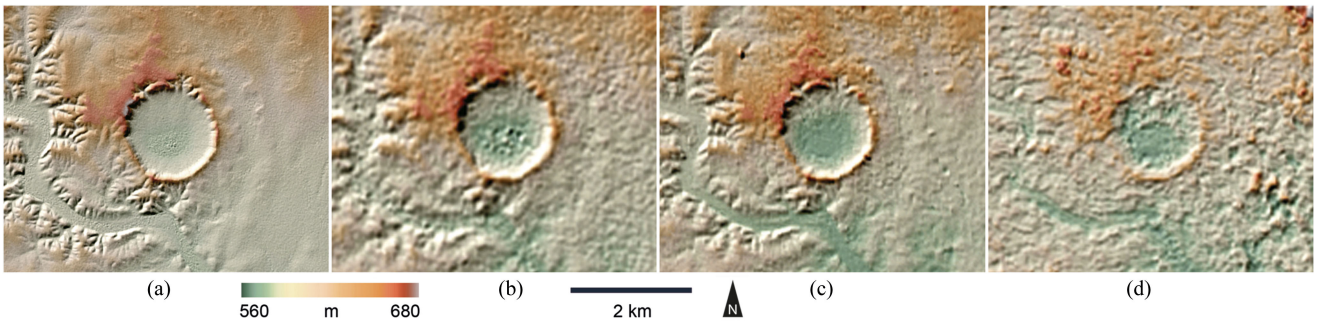

Fig. 12. Center of Fig. 11 with the Talemzane impact crater, displayed at identical resolution with (a) TanDEM-X, (b) SRTM, (c) ALOS, and (d) ASTER. The color-coded hillshaded map was produced from the corresponding DEMs using the same workflow.

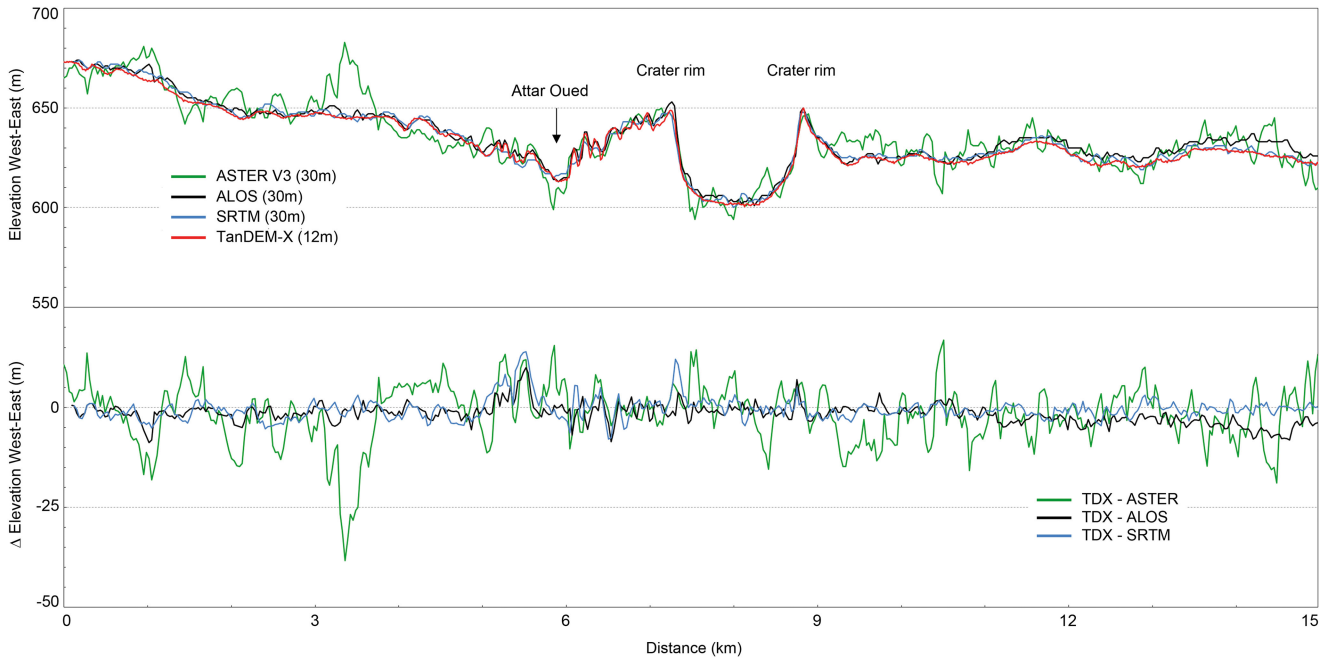

Fig. 13. West-east transect through the Talemzane impact crater based on four space-borne DEMs. The top display shows the elevation profile, whereas the bottom display indicates the elevation differences compared to TanDEM-X, which was resampled to a pixel posting of 30 m.

the larger crater pits are obvious in the physical map generated from the TanDEM-X DEM (see Fig. 15). The double crater with an overall extent of 180 m is most prominent, but also smaller structures with diameters down to 60 m can be identified.

More difficult becomes the detection of very small craters in the presence of dense vegetation that would shield them from TanDEM-X's radar pulses. This is particularly true for the European crater fields at Ilumetsä, Kaalijärv, and Morasko. In each of these crater fields, the main crater pit has a diameter of 80, 110, and 96 m. Only their main crater pits are poorly visible in the corresponding TanDEM-X maps. An example is given for the Morasko crater field where the main pit forms a shallow indentation in the forested part of the scene (see Fig. 16). Over areas covered by uniformly distributed dry sand with small grain size, radar backscatter is low and the DEM derived from these data becomes less accurate. Therefore, even the largest of the shallow Wabar craters with a diameter of 116 m in Saudi Arabia's Rub'al-Khalī desert could not be detected.

Of the 16 very small craters still visible in topography, the TanDEM-X DEM fails to detect only 7 of them (Campo del Cielo Crater Field in Argentina, Carancas in Peru, Dalgaranga in Australia, Sikhote Alin Crater Field and Sobolev, both in Russia, Wabar in Saudi Arabia, and Whitecourt in Alberta/Canada). The rest (Boxhole in Australia, Douglas Crater Field in Wyoming/USA, Henbury Crater Field in Australia, Kamil in Egypt, Ilumetsä Crater Field and Kaalijärv Crater Field, both in Estonia, Morasko Crater Field in Poland, Odessa Crater Field in Texas/USA, and Veevers in Australia) is obvious—in crater fields at least with their main crater pit.

All of the remaining impact structures with diameters > 250 m can be mapped with the TanDEM-X DEM, and morphologic properties can be retrieved with significance from this dataset.

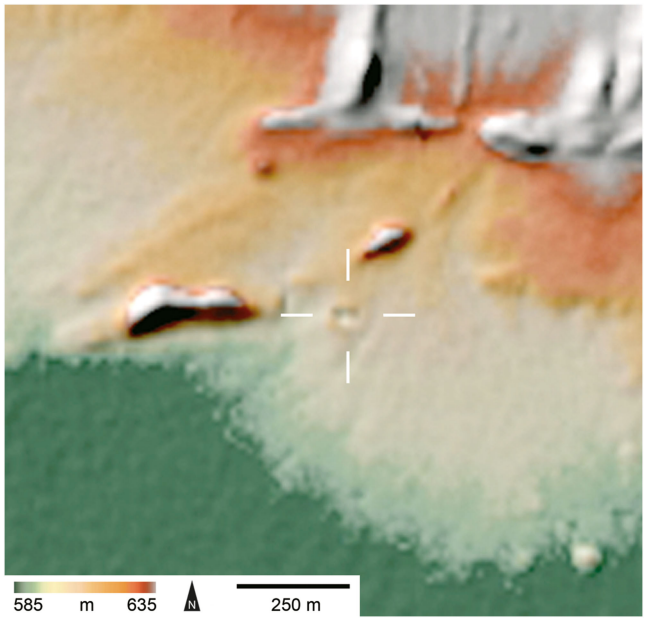

Fig. 14. Kamil impact crater with a diameter of only 45 m (indicated by cross hairs) in a color-coded hillshaded TanDEM-X DEM.

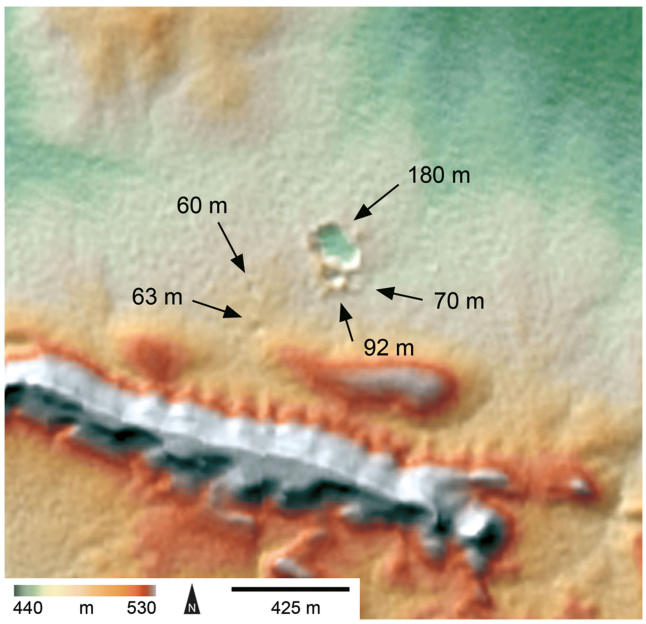

Fig. 15. Henbury crater field in a color-coded hillshaded TanDEM-X DEM. Several larger craters are indicated.

This gives, presently, more than 100 impact structures that can be precisely studied using the TanDEM-X DEM.

V. Conclusion

This article demonstrates what can be gained in the field of impact geology by using the TanDEM-X DEM for morphological studies. The global coverage of this DEM provides access to all presently confirmed structures, even those beyond the Arctic Circle. The high absolute and relative vertical precision, combined with the high spatial sampling, allows mapping of topographic fine structure. The results presented for a subsample of craters including a small simple crater and large complex structures demonstrate the strength of these data in comparison with other space-borne global DEMs. Our analysis indicates a lower diameter detection limit of some 50–100 m for impact craters in the TanDEM-X DEM in suitable terrain. Mapping structures of about 250 m diameter and larger already allows to evaluate reliable morphometric properties.

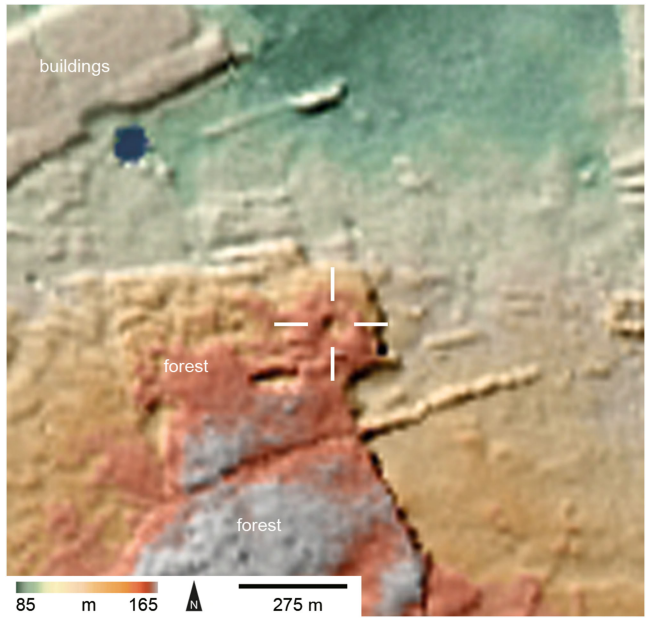

Fig. 16. Morasko crater field in Poland. Only the main crater pit is visible (indicated by cross hairs) in the forested area in the color-coded hill shaded TanDEM-X DEM.

Acknowledgment

The authors would like to thank the open access to the Copernicus Sentinel-2 data that ensured the generation of the combined TanDEM-X and multispectral RGB images.

References

[1] M. Gottwald, T. Kenkmann, and W. U. Reimold, *Terrestrial Impact Structures: The TanDEM-X Atlas, Vol. 1 and 2*. Munich, Germany: Verlag Dr. Friedrich Pfeil, 2020, pp. 608.
[2] B. M. French, *Traces of Catastrophe: A Handbook of Shock-Metamorphic Effects in Terrestrial Meteorite Impact Structures* (LPI Contribution 954). Houston, TX, USA: Lunar and Planetary Inst., 1998 , p. 120.
[3] S. P. Wright, L. L. Tornabene, and M. S. Ramsey, "Remote sensing of impact craters," in *Impact Cratering: Processes and Products*, G. R. Osinski and E. Pierazzo, Eds. Chichester, U.K.: Wiley-Blackwell, 2013, pp. 194–210.
[4] T. Kenkmann, M. Poelchau, and G. Wulf, "Structural geology of impact craters," *J. Struct. Geol.*, vol. 62, pp. 156–182, May 2014.
[5] B. P. Glass and B. M. Simonson, *Distal Impact Ejecta Layers*. Berlin, Germany: Springer-Verlag, 2013, p. 716.
[6] S. Hergarten and T. Kenkmann, "The number of impact craters on earth: Any room for further discoveries?," *Earth Planet. Sci. Lett.*, vol. 425, pp. 187–192, Sep. 2015.
[7] G. Krieger *et al.*, "TanDEM-X: A radar interferometer with two formation-flying satellites," *Acta Astronautica*, vol. 89, pp. 83–98, 2013.
[8] P. Rizzoli *et al.*, "Generation and performance assessment of the global TanDEM-X digital elevation model," *ISPRS J. Photogramm. Remote Sens.*, vol. 132, pp. 39–49, Oct. 2017.

[9] T. G. Farr *et al.*, "The shuttle radar topography mission," *Rev. Geophys.*, vol. 45, no. RG2004, pp. 1–33, Jun. 2007.
[10] T. Tadono *et al.*, "Generation of the 30 m-mesh global digital surface model by ALOS PRISM," *Int. Arch. Photogramm., Remote Sens. Spatial Inf. Sci.*, vol. XLI-B4, pp. 1345–1352, Jul. 2016.
[11] M. Abrams *et al.*, "The advanced spaceborne thermal emission and reflection radiometer (ASTER) after fifteen years: Review of global products," *Int. J. Appl. Earth Observ. Geoinf.*, vol. 38, pp. 292–301, Jun. 2015.
[12] R. A. F. Grieve, *Impact Structures in Canada*, 2006.
[13] T. Kenkmann, M. A. R. Vasconcelos, A. P. Crósta, and W. U. Reimold, "The complex impact structure Serra da Cangalha, Tocantins State, Brazil," *Meteoritics Planet. Sci.*, vol. 46, no. 6, pp. 875–889, Jun. 2011.
[14] W. U. Reimold, G. R. J. Cooper, R. Romano, D. R. Cowan, and C. Koeberl, "Investigation of shuttle radar topography mission data of the possible impact structure at Serra da Cangalha, Brazil," *Meteoritics Planet. Sci.*, vol. 41, no. 2, pp. 237–246, Feb. 2006.
[15] W. U. Reimold and C. Koeberl, "Impact structures in africa: A review," *J. Afr. Earth Sci.*, vol. 93, pp. 57–175, May 2014.
[16] J. F. McHone and R. Greeley, "Talemzane: Algerian impact crater detected on SIR-A orbital imaging radar," *Meteoritics*, vol. 22, pp. 253–264, Sep. 1987.
[17] M. Gottwald, T. Fritz, H. Breit, B. Schättler, and A. Harris, "Remote sensing of terrestrial impact craters: The TanDEM-X digital elevation model," *Meteoritics Planet. Sci.*, vol. 52, no. 7, pp. 1412–1427, Jul. 2017.
[18] A. Gruber, B. Wessel, M. Huber, and A. Roth, "Operational TanDEM-X DEM calibration and first validation results," *ISPRS J. Photogramm. Remote Sens.*, vol. 73, pp. 39–49, Sep. 2012.
[19] A. Gruber, B. Wessel, M. Martone, and A. Roth, "The TanDEM-X DEM mosaicking: Fusion of multiple acquisitions using InSAR quality parameters," *IEEE J. Sel. Topics Appl. Earth Observ. Remote Sens.*, vol. 9, no. 3, pp. 1047–1057, Mar. 2016.

Manfred Gottwald received the Diploma degree in physics from the Ludwig-Maximilians-Universität, Munich, Germany, in 1978 and the Ph.D. degree from the Technical University Munich, Munich, Germany, in 1983.

After his Ph.D., he worked in high-energy astrophysics for the European Space Agency and the Max-Planck Institute for Extraterrestrial Physics. From 1991 to September 2018, he was with the German Aerospace Center, Wessling, Germany. At the Remote Sensing Technology Institute, he was involved in many space-borne missions investigating our atmosphere and our cryosphere. His responsibilities included, e.g., managing operations of the atmospheric science mission SCIAMACHY on the European ENVISAT platform and coordination of the National Earth Observation Missions in support of polar science under the auspices of the World Meteorological Organization for the International Polar Year 2007/2008 and beyond. When initial TanDEM-X DEM results became available, he began studying terrestrial impact structures using these data. Together with Thomas Kenkmann and Wolf Uwe Reimold, he has recently published the first topographic atlas of all confirmed terrestrial impact structures based on the final TanDEM-X DEM.

Thomas Kenkmann studied geology and paleontology at the University of Cologne and received the Ph.D. degree from Freie Universität Berlin, Berlin, Germany, in 1997.

Since 2010, he has been a Professor of geology and structural geology with the University of Freiburg, Breisgau, Germany, where he and his working group are investigating the structure and deformation inventory of impact craters on Earth and other planetary bodies at scales ranging from satellite imagery to micrometers. He is a passionate field geologist, who has studied more than 40 terrestrial impact craters worldwide, mapped many of them geologically, and is responsible for a number of crater discoveries and confirmations. He is also an experimentalist and initiated and coordinated a multidisciplinary consortium to understand meteorite impact into various rock types by conducting shock and cratering experiments.

Dr. Kenkmann was the recipient of the Barringer Medal and Award of the Meteoritical Society for his key contributions to the areas of impact crater research.

Wolf Uwe Reimold received the M.Sc. and Ph.D. degrees from the University of Münster, Münster, Germany, in 1977 and 1980, respectively, both in mineralogy.

From 1984 to 2005, he had a professorship in mineralogy at the University of Witwatersrand, Johannesburg, South Africa. From 2006 to 2018, he was a Professor of mineralogy and petrography with Humboldt Universität zu Berlin and then the Head of the Research Division "Evolution and Geoprocesses," Naturkunde Museum, Berlin, Germany. In 2018, he took retirement in Berlin, and a new position as a Professor Titular with the Institute of Geosciences, University of Brasilia, Brasilia, Brazil. His main research interests include multidisciplinary impact crater and shock metamorphism studies, where impact research was mainly focused on structures in Africa, Europe, North America, and, in recent years, Brazil, including a major contribution to the understanding of the Vredefort impact structure in South Africa.

Dr. Reimold was the recipient of the Barringer Medal and Award by The Meteoritical Society for his impact cratering research.

Thomas Fritz received the Diploma degree in physics from the University of Münster, Münster, Germany, in 1996 and the Ph.D. degree in astronomy from the University of Bonn, Bonn, Germany, in 2000.

He held a postdoctoral position with the Radioastronomical Institute, University of Bonn. In 2003, he joined German Aerospace Center, Wessling, Germany, and participated in the development of the TerraSAR-X multimode synthetic aperture radar (SAR) processor. In particular, he was responsible for the TerraSAR-X SAR product specification. Since 2008, he has been leading the development of the bistatic interferometric SAR processing chain for the TanDEM-X mission. He is currently the leader of the team "New SAR Applications" at the Remote Sensing Technology Institute, where he is involved in processing chain designs for future SAR missions. His research interests include geodetic and geophysical SAR applications, SAR and InSAR algorithms, and SAR topography.

Helko Breit received the Diploma degree in electrical and telecommunication science from the Technical University of Munich, Munich, Germany, in 1990.

Since 1990, he has been with German Aerospace Center, Wessling, Germany, where he is supervising the synthetic aperture radar (SAR) processor development team at the Remote Sensing Technology Institute. He has worked on a variety of international missions, including SIR-C, X-SAR and SRTM/X-SAR. He also contributed to several European Space Agency studies and supported the commissioning of the ESA's Sentinel 1 SAR satellites. Particularly challenging were the German missions TerraSAR-X and TanDEM-X where he was responsible for the development of the TerraSAR-X multimode SAR processor (TMSP) and the bistatic processing of TanDEM-X mission data. His research interests include the development of SAR processing algorithms and systems for future SAR satellites and missions.